FEMTOSECOND LASER STUDIES OF CO AND NO ON Pd(111)

A thesis submitted for the degree of

Doctor of Philosophy

Jadranka Butorac

October 2011

University College London

I, Jadranka Butorac, confirm that the work presented in this thesis is my own. Where information has been derived from other sources, I confirm that this has been indicated in the thesis.

You leave home to seek your fortune and, when you get it, you go home and share it with your family.

To Zoran, Dorotea, Vjeko and Jelisaveta

ABSTRACT

The ultimate goal of any branch of chemistry, including surface chemistry, is to understand the dynamics of reactions. The typical time scale for bond making and breaking is the femtosecond time scale. Femtochemistry has led to enormous progress in the understanding, and even control, of chemical reactions in the gas and solution phases over the past decades. However, a comparable level of sophistication in the analysis of surface chemical reactions has not been achieved due to the complexity of the energy dissipation channels. For this thesis, a new experimental set-up was built with the goal to monitor the femtosecond laser-induced desorption (fs-LID) and femtosecond laser-induced reaction (fs-LIR) of CO and NO co-adsorbed on a Pd(111) surface. In addition, a femtosecond extreme ultraviolet (XUV) source was designed and commissioned. All the femtosecond laser-induced studies were accompanied by temperature programmed desorption (TPD) and reflection absorption infrared spectroscopy (RAIRS). First, fs-LID experiments were performed for pure CO and NO adsorbed on Pd(111) in order to test the apparatus. The CO and NO photodesorption dynamics were compared and the different photoreactivity was explained qualitatively using two theoretical models: electron friction and desorption induced by multiple electronic transitions (DIMET). The power law behaviour was also tested and a new method of fitting proposed. The photodesorption behaviour of CO co-adsorbed with NO on Pd(111) was then studied and compared qualitatively with the photodesorption behaviour of pure CO and NO within the empirical friction model.

The work described in this thesis is being prepared for submission for publication.

Chapter 4

The photochemistry of NO and CO on Pd(111)
J. Butorac, R.S. Minns, E. L. Wilson, H. H. Fielding and W. A. Brown
To be submitted to *J. Phys. Chem. C.*

The photochemistry of the NO/Pd(111) and CO/Pd(111) systems has been investigated as a function of surface coverage using femtosecond laser-induced desorption (fs-LID) and compared with temperature programmed desorption. The adsorbate-surface systems are characterised using RAIRS. The fs-LID yield is monitored as a function of surface coverage and laser fluence. A new fitting procedure is proposed to take into account the threshold for laser-induced desorption.

Chapter 5

Femtosecond laser-induced desorption of NO + CO on Pd(111)
J. Butorac, E. L. Wilson, R.S. Minns, W. A. Brown and H. H. Fielding
To be submitted to *J. Phys. Chem. C.*

The photochemistry of NO+CO on Pd(111) has been investigated as a function of surface coverage using femtosecond laser-induced desorption (fs-LID) and compared with temperature programmed desorption. The fs-LID yield is monitored as a function of surface coverage and laser fluence.

ACKNOWLEDGEMENTS

The work presented in this thesis was supervised by Helen Fielding and Wendy Brown to whom I express my gratitude for their advice, encouragement and active assistance. Helen Fielding was very supportive at the start of my PhD. She had great ideas how to solve either theoretical or practical problems and how to raise my spirit in the case of any accidents. Wendy was very helpful in the lab, and with time management. Thanks to both of them for their fast and thorough reading of my thesis chapters. I would also like to take this opportunity and express my gratitude to the EPSRC, ORS, Global Excellence Scholarship and Horswill Bequest for the provision of a studentship, without which none of this would have been possible.

I thank Professor Peter Saalfrank who provided me with some very useful ideas for Chapter 4 and Dr. Steve Firth who helped me deal with the femtosecond laser system. I am indebted to Dr. Russell Minns for his patience and his readiness to answer all my questions, and to his wife, Katherine, who read the first versions of my result chapters and helped me with the English. I am also indebted to Dr. Emma Wilson who taught me everything I know about the UHV system.

Many thanks to the staff and research students at UCL especially Ciarán, Roman, Douglas, Abi, Dorian, Maria, Adam K, Adam M, Jon, Nick and Rakhee, and to the staff in the MAPS faculty workshops, especially Roy and Jim. I would also like to thank Dave Knapp for help with the rotary pumps, and Len Parrish for all his assistance in synchronizing the femtosecond laser system and quadrupole mass spectrometer.

I would like to express my gratitude to my family, especially my mother, mother-in-law, sister Marija and sisters-in-law Anja and Mira for their help with looking after my son, Zoran, whilst I wrote this thesis. Finally I would like to thank my husband Vjeko and my children Zoran and Dorotea, without whose love and support I would have never gone this far.

CONTENTS

LIST OF FIGURES

CHAPTER 1

CHAPTER 2

CHAPTER 3

CHAPTER 4

CHAPTER 5

LIST OF TABLES

CHAPTER 1

CHAPTER 2

CHAPTER 4

CHAPTER 5

FREQUENTLY USED ABBREVIATIONS

2PC	two pulse correlation
CCD	charge coupled device
CPA	chirped pulse amplification
cw	continuous wave
DFT	density functional theory
DIET	desorption induced by electronic transitions
DIMET	desorption induced by multiple electronic transitions
DOS	density of states
fs-LID	femtosecond laser-induced desorption
fs-LIR	femtosecond laser-induced reaction
FTIR	Fourier transform infrared
FWHM	full-width at half maximum
GDD	group delay dispersion
GVD	group velocity dispersion
HOMO	highest occupied molecular orbital
HREELS	high resolution electron energy loss spectroscopy
IR	infrared
L	Langmuir
LEED	low energy electron diffraction
LUMO	lowest occupied molecular orbital
MCT	mercury cadmium telluride
ML	monolayer
PES	potential energy surface
PM	polarisation modulation
QMS	quadrupole mass spectrometer
RAIRS	reflection absorption infrared spectroscopy
REMPI	resonance enhanced multiphoton ionization
SFG	sum frequency generation
SHG	second harmonic generation
STM	scanning tunnelling microscopy
TPD	temperature programmed desorption

TRPES	time-resolved photoelectron spectroscopy
TTL	transform transform limited
UHV	ultra high vacuum system
UPS	ultraviolet photoemission spectroscopy
UV	ultraviolet
XUV	extreme ultraviolet
yield-FD	fluence dependence of the reaction yield

CHAPTER 1

INTRODUCTION

Surfaces are known to be very difficult systems to study, due to complex surface preparation procedures, and the requirement to maintain a clean and well-defined surface. However, detailed understanding of chemical reactions on metal surfaces is particularly important since many metal surfaces are known to be good catalysts for a large number of chemical reactions. The ultimate goal is to understand the *dynamics* of surface reactions and this is not possible by simply utilizing standard surface science techniques such as scanning tunnelling microscopy (STM), low energy electron diffraction (LEED), high resolution electron energy loss spectroscopy (HREELS), ultraviolet photoelectron spectroscopy (UPS), temperature programmed desorption (TPD), reflection absorption infrared spectroscopy (RAIRS), and many others.

In order to be able to elucidate the dynamics of chemical reactions on surfaces, femtosecond time resolution is necessary, since this is the timescale of bond making and bond breaking. Experimental studies with femtosecond time resolution became possible with the development of lasers with ultrashort pulse duration. [1] The field was pioneered by Zewail and co-workers and recognized by the award of the Chemistry Nobel prize in 1999.[2] Time-resolved femtochemistry experiments led to huge progress in the understanding and control of chemical reactions in the gas and solution phase, however surface femtochemistry, both static and time-resolved, is still in relative infancy, with the fundamental processes not well-understood.

In this thesis, a novel experimental set-up is designed in order to monitor, for the first time, the femtosecond laser-induced desorption (fs-LID) and reaction of CO and NO co-adsorbed on a Pd(111) surface.

1.1 Motivation for studying adsorption of CO and NO on surfaces

The study of the adsorption of molecules on solid surfaces has increased greatly since the early 1960s. About 90% of all industrial chemical processes involve heterogeneous catalysis, which is not only the basis of the chemical and petroleum industries, but is also of crucial importance for protecting the environment. [3]

In this PhD thesis, the reaction of interest is that between CO and NO on Pd(111). The CO + NO reaction has been studied over a variety of transition and noble metal catalysts. [4 –13] In the late 1970s, the three-way catalytic converter was introduced into the emission control systems of car exhausts in the United States. The three-way catalytic converter simultaneously catalyses three reactions: the reduction of NO_x species, the oxidation of CO and the oxidation of excess hydrocarbons, as shown in Scheme 1.1.

$$2NO_x \rightarrow xO_2 + N_2 \quad (1)$$

$$2CO + O_2 \rightarrow 2CO_2 \quad (2)$$

$$C_xH_{2x+2} + [(3x+1)/2]O_2 \rightarrow xCO_2 + (x+1)H_2O \quad (3)$$

Scheme 1.1. Reactions in the three-way catalytic converter.

In order to choose the cheapest and the best catalyst it is important to understand the fundamental reaction pathways and catalytic characteristics. The first catalysts were made of platinum and rhodium (90% platinum and 10% rhodium). The problem with these catalysts is that rhodium is expensive and a rare element, so with the increasing number of cars in operation there is a desire to replace rhodium with a less expensive, more plentiful, substitute. Palladium is one possible alternative, not only because it is more plentiful, but it has also been found to be more durable at higher reaction temperatures, so it can be positioned nearer to the engine. Palladium has also demonstrated excellent hydrocarbon oxidation characteristics. [3]

1.2 Surface science approach in studying real catalysts

A typical catalyst consists of nanometer sized particles with a lot of different crystal planes with various structural defects and chemisorbed foreign atoms. Hence, the surface chemistry of a real catalyst is rather complex. [14] Langmuir [15] in 1922 suggested a scientific approach that enables studying real catalysts in a systematic way:

In order to simplify our theoretical considerations of reactions at surfaces, let us confine our attention to plane surfaces. If the principles in this case are well understood, it should then be possible to extend the theory to the case of porous bodies.

Thus, the first step towards understanding reactions on real surfaces that are used in catalysis is to understand the reaction on a well-defined, single-crystal surface that is prepared and investigated using ultrahigh vacuum (UHV) techniques and a whole range of classic surface science techniques. Since most classic surface science techniques cannot be performed at the high pressure conditions of real catalysis, there is a so-called 'pressure gap'. In addition, since the properties of well-defined single crystal surfaces will generally be quite different to the surface properties of real catalysts, there is a so-called 'materials gap'. [14] The materials gap can be overcome by comparing reactions on various well-defined surfaces with conventional high surface area powder catalysts. [3] Some of the surface science techniques, such as RAIRS, can be used under atmospheric conditions. Hence, the pressure gap can be overcome by studying the reaction at different pressures.

In this thesis, the reaction of interest is studied on a well-defined, single crystal surface under UHV conditions as a first step towards understanding the same reaction on real catalysts under atmospheric conditions.

1.3 Importance of femtosecond lasers in surface photochemistry

There are several factors motivating the use of femtosecond lasers in surface science experiments. Perhaps the most obvious motivation, as in gas-phase studies, [16, 17] is the possibility of direct access to the fundamental time-scale of the relevant chemical processes. In addition to this, the absorption of femtosecond laser pulses at a metal surface can result in the creation of unique, non-equilibrium, excitation of the substrate. The exploration of surface processes resulting from these conditions is interesting in its

own right. Figure 1.1 shows a flow chart of how energy can be transferred between the substrate and adsorbate electronic and vibrational excitations.

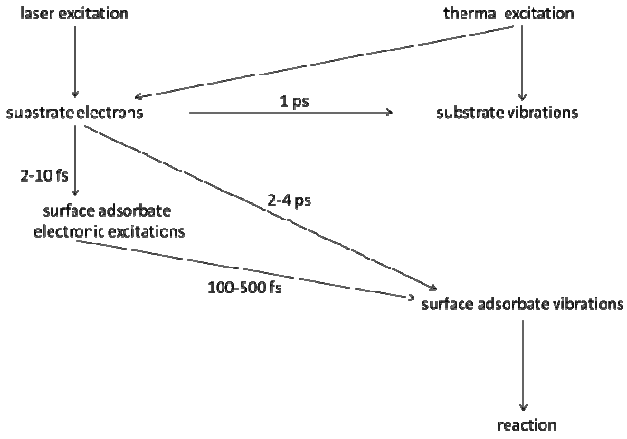

Figure 1.1 Chart of energy flow at electronic conductor surfaces excited by lasers *versus* conventional thermal sources.

All of the processes shown in Figure 1.1 can be identified in a time-resolved experiment. If the reaction finishes ~60 fs after the photoabsorption event, then there is probably a direct coupling between electronic excitations of the adsorbate-substrate complex and the surface adsorbate vibrations (the reaction will take ~10 fs within the electronic lifetime plus half a vibrational period, typically ~50 fs). However, if the substrate electrons excite the adsorbate surface vibration non-resonantly, then the reaction may not begin for ~1 ps, because the coupling time between the substrate electrons and the vibrations is ~1 ps. In the case of substrate phonons exciting adsorbate surface vibrations, the reaction will be finished in more than 10 ps. From these examples, it is clear that the reaction-time provides a direct way of distinguishing between different pathways.

The mechanism of energy flow between an adsorbate and a substrate is of fundamental importance in surface science. The role of coupling of the adsorbate motion to the substrate phonons is well understood, but the influence of energy exchange with substrate electronic excitations under thermal conditions has been the subject of discussion for many years. [18 – 21] These effects are especially important in chemisorbed systems, where there is a charge transfer between the substrate and the adsorbate.

Irradiation of a metal surface with femtosecond laser pulses results in the confinement of all energy in the electronic system during short-lived, electron-hole pair transients. These non-thermalized, hot carriers are capable of inducing surface reactions. This effect is the well-known process of substrate mediated surface photochemistry. However, in classic substrate mediated surface photochemistry (using a continuous wave laser or a nanosecond pulse laser) the density of these hot carriers is usually low, so the possibility for new reaction channels is not as high as with femtosecond laser pulses.

Femtosecond laser pulses also enable the study of non-adiabatic effects. When the substrate is a metal surface, there is a whole manifold of electron-hole pair excitations, so the Born-Oppenheimer (adiabatic) approximation is often not a good approximation. The Born-Oppenheimer approximation assumes that the electron motion is much faster than the nuclear motion, hence the electrons adjust instantaneously to the current nuclear configuration. When the electrons do not respond instantaneously to the motion of the adsorbate, electron-hole pairs can be created or destroyed, and this is the origin of strong non-adiabatic couplings.

1.4 Laser excitation of a metal adsorbate system

In Figure 1.1 it was shown schematically how energy flows between the electronic and vibrational excitations in the adsorbate-substrate complex and several pathways by which laser excitation can lead to chemical reaction. Each of these subsystems can be studied in detail. Hence, first the response of the metal substrate (parameters will be given for Pd(111)) to femtosecond laser pulses will be considered and then the electronic structures of the adsorbates, CO and NO, on Pd(111) will be presented. Finally, two models for describing the coupling mechanism for the energy transfer between the substrate and adsorbate will be described.

1.5 Laser excitation of the substrate

Upon photoabsorption, the following processes occur within a metal substrate: [22]

1) Photons of energy *hv* are absorbed by the electrons.

2) The non-equilibrium electron distribution relaxes by electron-electron interactions toward the Fermi-Dirac distribution, which can be characterized by a local electron temperature $T_e(r, t)$.

3) Simultaneously with **2)**, electrons scatter to lower energies by electron-phonon interactions. The resulting excited phonons are not necessarily in thermal equilibrium with the electrons.

4) The non-equilibrium phonon distribution relaxes by phonon-phonon and electron-phonon interactions toward the equilibrium Bose-Einstein distribution at the local lattice temperature $T_p(r, t)$.

5) Simultaneously with **1)** to **4)**, thermal diffusion, carried by the electrons, distributes the energy deposited within the optical penetration depth into the bulk.

As an approximate description of the substrate excitation, the two temperature model [23] is usually used. In this model, the electronic excitation is taken to be characterized by an equilibrium Fermi-Dirac distribution at a temperature T_e (electron heat bath) and the phonons are characterized by a thermal Bose-Einstein distribution at a temperature T_p (phonon heat bath). The electron heat bath transfers energy, either to the substrate by thermal diffusion, or to the phonon heat bath *via* electron-phonon coupling. In this model, only one-dimensional heat flow along the surface normal direction z will be considered, since the size of the laser spot is large compared to the optical penetration length and the lateral thermal diffusion lengths. The temporal evolution of the electron and phonon heat baths can be represented by a set of coupled differential equations:

$$C_e \frac{\partial T_e}{\partial t} = \frac{\partial}{\partial z} \kappa_e \frac{\partial T_e}{\partial z} - g(T_e - T_p) + A(z,t) \qquad (1.1a)$$

$$C_p \frac{\partial T_p}{\partial t} = g(T_e - T_p), \qquad (1.1b)$$

where C_e and C_p denote, respectively, the electronic and phonon heat capacities, κ_e is the thermal conductivity, g is the electron-phonon coupling constant, and $A(z, t)$ represents a term which is due to the absorption of the laser pulse. All the constants necessary to solve these equations for Pd are given in Table 1.1.

Table 1.1 Physical properties of palladium.

electronic specific heat coefficient	γ_1	249.14 J m^{-3} K^{-2} [24]
electronic specific heat offset	γ_0	249.14 J K^{-2} m^{-3}
thermal conductivity at 300 K	κ_0	72 W m^{-1} K^{-1} [25]
Debye temperature	ϑ_D	274 K [25]
refractive index (800 nm)	n_r+ik	2.08+4.55*i*
optical penetration depth*	δ	14 nm

The temperature dependence of the electron thermal conductivity can be approximated *via*: [26]

$$\kappa_e = \kappa_0 \frac{T_e}{T_p}, \tag{1.2}$$

where κ_0 is the thermal conductivity at 300 K (given in Table 1.1).

The phonon heat capacity, as a function of phonon temperature T_p, can be calculated according to the Debye approximation: [25]

$$C_p = 9N_A k_B \left(\frac{T_p}{\vartheta_D}\right)^3 \int_0^{\frac{\vartheta}{T_p}} dx \frac{x^4 e^x}{\left(e^x - 1\right)^2}, \tag{1.3}$$

where N_A is the Avogadro constant, k_B is the Boltzmann constant and ϑ_D is the Debye temperature that is given in Table 1.1. For $T_p > \vartheta_D$, Equation 1.3 passes into the Dulong-Petit law, where a constant heat capacity, C_p ~25 J K^{-1} mol^{-1} is derived.

The heat capacity of the electrons, C_e, depends on T_e and is given by [25]

$$C_e = \gamma_0 + \gamma_1 T_e, \tag{1.4}$$

where γ_1 is the electronic specific heat coefficient and γ_0 is the electronic specific heat offset, both given in Table 1.1.

The value of the electron-phonon coupling constant, $g = 5\times10^{11}$ W cm^{-3} K^{-1}, was determined from the relationship given by Allen. [27]

The overall optical excitation *A*, as a function of *z* and *t* is:

---

* $\delta = \frac{\lambda}{4\pi k}$, where λ is the wavelength and *k* is the imaginary part of refractive index.

$$A(z,t) = \frac{(1-R)I(t)}{\delta}\exp\left(-\frac{z}{\delta}\right), \tag{1.5}$$

where R is the reflectivity of the metal surface for the particular angle of incidence, I is the intensity of laser radiation, z is the direction of propagation perpendicular to the surface, and δ is the optical penetration depth. The reflectivity for light polarized perpendicular (R_s) or parallel (R_p) to the plane of incidence can be calculated from the Fresnel equations as a function of the angle of incidence i: [28]

$$R_s = \frac{a^2 + b^2 - 2a\cos i + \cos^2 i}{a^2 + b^2 + 2a\cos i + \cos^2 i} \tag{1.6a}$$

and

$$R_p = R_s \frac{a^2 + b^2 - 2a\sin i\tan i + \sin^2 i\tan^2 i}{a^2 + b^2 + 2a\sin i\tan i + \sin^2 i\tan^2 i}, \tag{1.6b}$$

where a, b can be obtained from

$$2a^2 = [(n_r{}^2 - k^2 - \sin^2 i)^2 + 4n_r{}^2k^2]^{1/2} + (n_r{}^2 - k^2 - \sin^2 i) \tag{1.6c}$$

$$2b^2 = [(n_r{}^2 - k^2 - \sin^2 i)^2 - 4n_r{}^2k^2]^{1/2} + (n_r{}^2 - k^2 - \sin^2 i). \tag{1.6d}$$

In these relations, n_r is the real part of the refractive index and k is the imaginary part of the refractive index, $n = n_r + \mathrm{i}k$.

In Chapter 5, qualitative analysis of photodesorption results for co-adsorbed systems is performed using results for T_e and T_p from Szymanski *et al.*[29], so all the physical constants and parameters needed to solve equations 1.1a and 1.1b are described in detail. Equations 1.6a and 1.6b are not only relevant for the calculation of the optical excitation in the two temperature model, but also for the calculation of absorbed laser fluence (described in detail in Chapter 2). For all experiments performed in this thesis, laser light was polarized perpendicular to the plane of the sample (parallel to the plane of incidence).

1.6 Electronic structure of the CO and NO on transition metals

In the free CO molecule, the 5σ and 2π* molecular orbitals are the highest occupied (HOMO) and lowest unoccupied (LUMO) molecular orbitals, respectively. Upon adsorption, it is generally assumed that the major CO-metal interaction can be explained in terms of interactions of the HOMO and LUMO of the adsorbate with the metal d-orbitals. The Blyholder model [30] is based on donation from the occupied CO 5σ orbital into empty surface orbitals, and back-donation from occupied surface orbitals to the unoccupied CO 2π* orbital. In the literature, there is divided opinion about this model. [31, 32, 33, 34] The chemisorption of CO on a metal surface can also be determined using density functional theory (DFT) calculations, [35] and the contribution to chemisorption is considered to be not only from the 5σ and 2π* orbitals, but also from the 1π and 4σ orbitals of CO.

Figure 1.2 shows the density of states (DOS) for the free CO molecule (for the 1π, 4σ, 5σ and 2π* orbitals) and the interaction of these orbitals with the metal substrate (Pt) d-orbitals. Based on the position of Pt and Pd in the periodic table, a similar interaction of CO with the Pd d-orbitals is expected. The position of the molecular orbitals of the CO adsorbate on Pd will be slightly shifted with respect to the Fermi level, since the Fermi energy of Pd is ~1 eV lower than the Fermi energy of Pt [36].

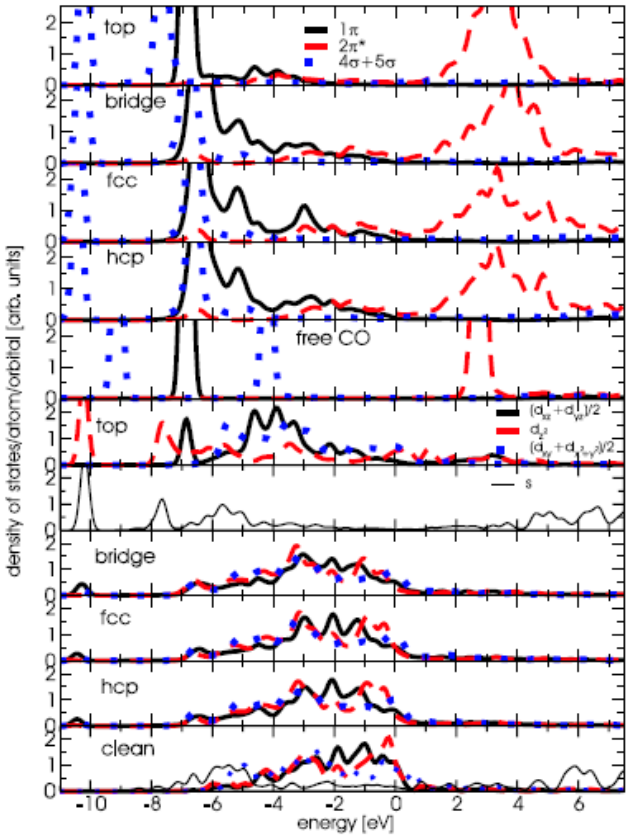

Figure 1.2 The electronic densities of states for the CO molecule adsorbed in top, bridge, fcc and hcp hollow sites of Pt surfaces. The upper five panels describe the density of states (DOS) for various molecular orbitals of the CO molecule. The lower six panels show the DOS for the substrate atom(s) interacting most with the molecule. The panels labelled "free CO" and "clean" describe the non-interacting case for comparison. Figure taken from reference 35.

The main role in bonding CO to the metal surface is due to the interaction of the 5σ, 1π and 2π* orbitals with the metal. Upon adsorption, these orbitals shift in energy and broaden. This broadening and shift increases with the coordination number of the substrate atoms. The 5σ orbital of CO interacts with the d_z^2 orbital of the metal, and the bonding contribution is centred ~7.5 eV below the Fermi level. [37] The antibonding contribution is located at higher energies and extends up to the Fermi level. The 1π and 2π* orbitals of CO interact with the d_{xz} (d_{yz}) and in plane ($d_{x^2-y^2}$, d_{xy}) orbitals of metal atoms. The main part of the 1π orbital is centred ~ 6 eV below the Fermi level. Upon adsorption, this peak broadens, ending up at the Fermi level. The partially filled 2π* orbital has a bonding contribution in the same energy range as the 1π orbital, but the

density of states is very low, as can be seen in Figure 1.2. The main antibonding contribution is positioned at ~3 eV above the Fermi level. [37]

The same mechanisms dominate the adsorption of NO, but now the partially filled $2\pi^*$ orbital, after interaction with the metal d-orbitals, has both bonding and antibonding contributions near the Fermi edge, and the 5σ and 1π orbitals are located at higher binding energies. The repulsive interactions arising from the interaction of the 1π orbital with the d-band are greatly reduced, while donation from the 5σ state is still efficient. [37] This electronic structure of the adsorbate substrate complex explains the larger adsorption energy of NO compared to CO, which is illustrated in TPD and RAIRS experiments in Chapters 4 and 5. Experimental investigations using direct and inverse photoelectron spectroscopy for CO and NO adsorption on Pd(111), show that the $2\pi^*$ orbitals of CO lies at around 4.6 eV with respect to the Fermi level, and the $2\pi^*$ orbitals of NO have contributions below the Fermi level (~-2.7 eV) and above the Fermi level (~1.7 eV), [38] in agreement with DFT calculations shown in Figure 1.2. The position of the $2\pi^*$ orbital with respect to the Fermi level gives one of the possible explanations for the lower fluence threshold for NO on Pd(111) than for CO on Pd(111) in terms of desorption induced by multiple electronic transitions (DIMET). This mechanism is explained in more detail in Section 1.8 b. The fluence threshold observed in fs-LID studies of CO and NO on Pd(111) is discussed in Chapter 4.

1.7 Mechanisms of coupling of electronic excitation to adsorbate degrees of freedom

The coupling of electronic degrees of freedom to adsorbate motion has received a great deal of attention in the literature. [32, 39] In this section, two models are discussed that treat the strong coupling between the substrate electronic excitation and adsorbate modes: the friction model and DIMET.

1.7.1 Friction model

In this model, [40, 41] adsorbate motion is assumed to occur on a single potential energy surface. The interaction of the adsorbate with substrate electronic excitations, causes the motion on the potential energy surface to be perturbed. Figure 1.3 is a cartoon illustrating the electronic friction mechanism.

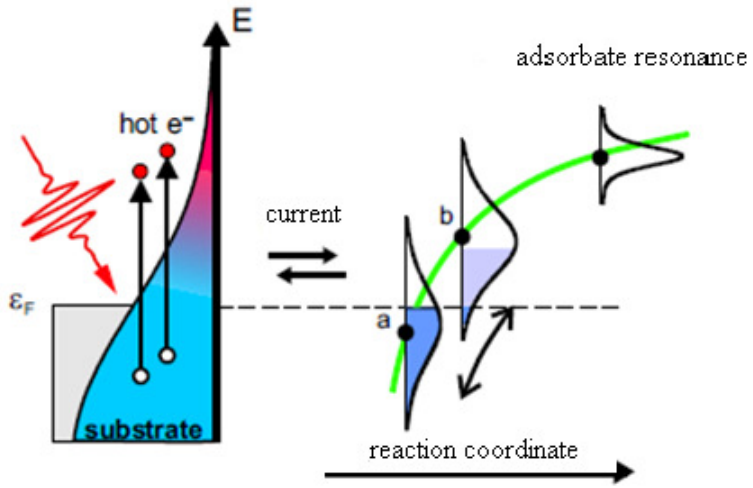

Figure 1.3 Frictional coupling between the adsorbate and the substrate. The adsorbate vibration leads to a motion along the reaction coordinate and an energetic shift of the adsorbate resonance with respect to the Fermi level. Motion of the adsorbate creates electron-hole pairs in the substrate. Figure taken from reference 42.

Two well-established models are used to describe the interactions of the adsorbate with substrate electronic excitations, one of which uses a quantum mechanical approach to describe the excitation of the intramolecular coordinate and the other uses classical equations to describe the motion of the centre of mass of the adsorbate.

1.7.1.1 Quantum mechanical approach to the friction model

In this model, the energy transfer between the substrate and the adsorbate is mediated by frictional coupling between the electron and phonon heat bath to a harmonic oscillator of the adsorbate motion. The time evolution of the energy content of the adsorbate is based on the master equation formalism, [40, 43] and can be represented by Equation 1.7: [44]

$$\frac{d}{dt}U_{ads} = \eta_e\left(U_e - U_{ads}\right) + \eta_p\left(U_p - U_{ads}\right) \qquad (1.7)$$

where η_e and η_p are coupling coefficients between the substrate electrons and the adsorbate and substrate phonons and the adsorbate, U_{ads} is the energy of the adsorbate and U_p and U_e denote the energy that would be in vibrations if it was equilibrated at a temperature T_p or T_e, respectively.

$$U_{p(e)} = \hbar\omega \left[\exp\left(\frac{\hbar\omega}{k_B T_{p(e)}} \right) - 1 \right]^{-1}, \tag{1.8}$$

where $\hbar$ is the Planck constant divided by 2π, ω is the angular frequency and k_B is the Boltzmann constant. If T_{ads}, T_p and $T_e >> \frac{\hbar\omega}{k_B}$, then the oscillator energies (U_{ads}, U_p and U_e) can be replaced by their classical limits - the corresponding temperatures themselves. Thus, Equation 1.7 becomes:

$$\frac{d}{dt} T_{ads} = \eta_e (T_e - T_{ads}) + \eta_p (T_p - T_{ads}). \tag{1.9}$$

T_{ads} can be calculated from Equation 1.9 after T_e and T_p are calculated using the two temperature model. [23] This T_{ads} is then used to obtain the reaction rate, R, and finally, the reaction yield, Y, as the time integral of R. The reaction rate is calculated from the Arrhenius expression for the desorption rate at a given oscillator temperature:

$$R(t) = -\frac{d}{dt}\theta = \theta^n \nu \exp\left(-\frac{E_a}{k_B T_{ads}(t)} \right), \tag{1.10}$$

where θ, n, ν and E_a denote the coverage, the order of the reaction kinetics, pre-exponential factor and activation energy for desorption. This model was used in Chapter 5 when desorption yields in fs-LID experiments of CO or NO in co-adsorbed systems are compared with desorption yields of pure CO or NO, respectively. In Chapter 4, the higher photoreactivity of NO is explained using the modified friction model developed by Brandbyge and co-workers. [41] In this model, only coupling between the substrate electrons and the adsorbate is considered, so Equation 1.9 becomes,

$$\frac{d}{dt} T_{ads} = \eta_e (T_e - T_{ads}). \tag{1.11}$$

The probability of desorption, P_{des}, in this model is given by Equation 1.12:

$$P_{des}(t) = E_a \int_0^\infty dt \frac{\eta_e}{T_{ads}} \exp\left(-\frac{E_a}{k_B T_{ads}} \right). \tag{1.12}$$

The activation energy, E_a, electron friction coefficient η_e, and adsorbate temperature T_{ads}, now enter the pre-exponential factor. It is very easy to relate a value of η_e to the

desorption probability, since the desorption probability is proportional to the value of the electron friction coefficient.

1.7.1.2 Classical treatment of motion in the friction model

The quantum mechanical model of electronic friction is only suitable for the case where the interaction potential is harmonic, for example, the excitation of the intramolecular vibration of the adsorbate. A semi-classical treatment of the motion enables the study of more complex and realistic potential energy surfaces, and gives direct information about the motion of the adsorbate-substrate complex. This approach has not been used in this thesis, but it will be described briefly as an approach from which information about the adsorbate-substrate system is obtained directly. The weakness of this model is in the error introduced by neglect of quantum mechanical effects. This error is not so significant for high electron temperatures where there is significant population of quantum states.

The nuclei are described by a classical equation of motion, with a frictional coupling to the heat bath. In its one-dimensional form, the Langevin equation [45] for motion is:

$$\frac{d^2z}{dt^2} + \eta_e \frac{dz}{dt} = \frac{F(z)}{m} + \Gamma(t). \qquad (1.13)$$

Here, m is the particle mass, z is the distance between the adsorbate and substrate, η_e is the friction coefficient for coupling between the electronic degrees of freedom of the substrate and the nuclear degrees of freedom of the adsorbate, F is the force acting on the particle in the adsorption well modelled by a Morse potential and $\Gamma(t)$ is the stochastic force. Direct integration of Equation 1.13 gives a set of stochastic trajectories of the adsorbate centre of mass coordinate.

1.7.2 DIMET

The DIMET model [46] is based on the model for desorption induced by electronic transitions [47] (DIET). In this model, the substrate electronic excitations act to induce electronic transitions in adsorbate localized states. It is employed in the literature for treating conventional photoinduced effects on surfaces [32, 39] induced by pulses of at least

picosecond duration. However, the novel aspect of this model associated with femtosecond pulses is related to the density of substrate electronic excitation (density of electron-hole pairs) seen at high electronic temperatures, T_e. This high density of electron-hole pairs can lead to a lot of successive electronic transitions that transfer energy into adsorbate motion before it vibrationally relaxes into the ground electronic state. Before introducing the DIMET model, the DIET model will be described briefly.

1.7.2.1 DIET model

The first successful explanation of the DIET mechanism was given by Menzel, Gomer and Redhead. [48, 49] The excitation mechanism is shown in Figure 1.4.

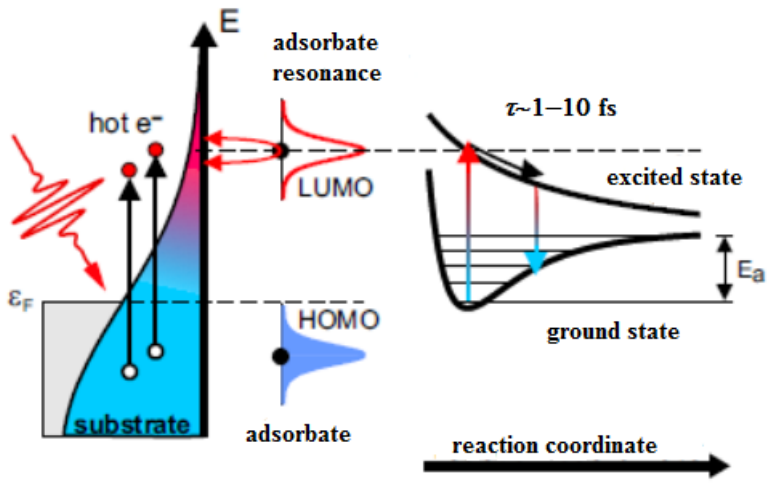

Figure 1.4 Schematic 1D illustration of DIET. Excitation of the adsorbate is through an electronic transition to a repulsive electronic state. After returning to the ground electronic state, the molecule gains vibrational energy. Figure taken from reference 42.

In Figure 1.4, the excited electronic state is repulsive, as proposed in the Menzel-Gomer-Redhead model. The same mechanism is also valid for bound excited states, first considered by Antoniewicz [50]. The ground potential energy surface (PES) can be described using a Morse potential. The system undergoes an electronic transition from the ground electronic state (HOMO) to the higher lying adsorbate resonance (LUMO). The equilibrium distance of the excited PES is displaced from that of the ground PES, so this results in a large force that accelerates the adsorbate towards the surface. The lifetime of the adsorbate on the excited PES is short, hence the adsorbate returns to the

ground PES after having moved only slightly, and usually the vibrational energy gain is not enough for the adsorbate to desorb. This fact explains the low desorption yields usually seen in DIET on metal surfaces.

1.7.2.2 DIMET model

At the high electronic temperatures reached during femtosecond laser irradiation of the substrate, a novel mechanism for the energy transfer between the substrate and adsorbate may appear. The initial step is a Franck-Condon transition to the excited PES. If the adsorbate remains on the excited PES for a time $t < \tau_c$ (τ_c is the minimum duration of motion on the excited PES necessary for desorption to occur), then the adsorbate cannot desorb, but it can make another Franck-Condon transition, from a vibrationally excited level of the ground PES. The adsorbate-surface vibration will therefore gain an additional amount of vibrational energy. A lot of these excitation-deexcitation cycles may occur within the lifetime of the molecule–surface vibration, so the desorption probability will be significantly enhanced compared to DIET. Stochastic trajectory simulations can be performed to obtain more quantitative understanding of the DIMET mechanism. For these simulations a knowledge of the ground and excited PES is required, as well as the rates of excitation and deexcitation. If the excited PES is regarded as a negative ion excited state, then the excitation and deexcitation can be regarded as the hopping of the electron from the substrate onto the adsorbed molecule and *vice versa*. The deexcitation rate can be modelled as:

$$k_d = \left[\tau^{-1} e^{-z/z_d}\right]\left[1 - f(\varepsilon_A(z), T_e(t))\right], \tag{1.14}$$

where τ is the excited state lifetime, z is the substrate-adsorbate distance, z_d is the parameter for the fall-off in the hopping rate, $f(\varepsilon, T_e)$ denotes the Fermi factor for energy ε and electronic temperature T_e. The activation rate can be modelled as:

$$k_a(z) = k_d(z) \exp\left[-\frac{\varepsilon_A(z)}{kT_e(t)}\right], \tag{1.15}$$

where k_d is the deexcitation rate, ε_A is the difference in the energy between the excited and ground PES for one value of z. The desorption trajectories can then be calculated

from stochastic simulations. In Chapter 4, the higher photoreactivity of NO compared to CO is explained using equations 1.14 and 1.15.

1.8 Link between laser-induced reactions and thermal reactions

The processes initiated by a femtosecond laser can be driven by non-equilibrium substrate electrons, before their thermal equilibration with phonons. A range of adsorbate/metal systems have been studied experimentally and theoretically using femtosecond laser excitation, see for example reference. [51]

If there is a possibility for competing reaction pathways, as was the case for O_2/Pt(111), [52] the channel favoured by thermally driven reactions can be different from the one favoured by femtosecond laser-induced reactions. In the case of O_2/Pt(111), heating of the Pt(111) surface with a saturation coverage of molecular oxygen gives rise to a substantial coverage of atomic oxygen, so the dissociation channel is preferred to the desorption channel. When the system is irradiated by femtosecond laser pulses, then there is a strong preference for desorption over dissociation. One of the exciting possibilities offered by femtosecond laser-induced reactions is the possibility for a new reaction path. This was demonstrated for a ruthenium surface on which carbon monoxide and atomic oxygen were co-adsorbed. [53] For this system, CO_2 cannot be formed thermally, but upon irradiation with femtosecond laser pulses there are two processes happening: formation of CO_2 (new reaction channel) and desorption of CO (a process also observed in thermally-induced reactions).

Nonetheless the reaction channels for thermally-induced desorption are sometimes the same as those for fs-LID. For example, based on the examples shown in the previous paragraph, it is expected that the dissociation channel will be active in the femtosecond laser irradiation of NO/Pd(111) [54] even though this is not the case in TPD experiments. There were no significant reaction products due to the molecular dissociation of NO, and this finding is consistent with the one from TPD.

There are many authors who have modelled fs-LID data successfully using activation energy from TPD data, either for the case where the channel favoured by a thermally driven reaction is different from the one favoured by fs-LID experiments (see for example Bonn *et al.* [53]) or is the same (see for example Prybyla *et al.* [54]).

In Chapter 5, the importance of finding a link between thermally-induced reactions and femtosecond laser-induced reactions is discussed. In the modelling of femtosecond laser-induced desorption by the friction approach, the desorption step can be modelled as the crossing of an effective activation energy barrier. If a simple one dimensional potential energy surface is assumed, then the activation energy for photoinduced desorption is presumed to be the same as that used to describe thermal desorption. There are several cases where the activation energy from TPD data has been used successfully to simulate photodesorption. [44,53,55,56] The photodesorption in these cases was modelled only for the case of one adsorbate on a particular metal surface. In this thesis a change in the position of the desorption peak maximum in TPD spectra in co-adsorbed (CO + NO/Pd(111)) with respect to the pure systems (CO/Pd(111) or NO/Pd(111)) is linked to the measured difference in the photodesorption yield for the first time.

1.9 Summary

This chapter introduced key topics that are important for the work described in Chapters 4 and 5. Chapter 4 describes the fs-LID of pure CO and NO on Pd(111) which have been performed before, [54, 56] providing a good test of the new apparatus. It also sets the scene for the next chapter. Chapter 5 describes the fs-LID of co-adsorbed CO and NO, together with a brief description of the reaction products generated during irradiation at one particular laser fluence.

The CO and NO reaction on Pd(111) was chosen because there is a lack of knowledge about the molecular mechanism. Palladium would be a good alternative to expensive rhodium that is currently used in car exhaust catalysis.

Irradiation of the CO(NO)/NO(CO)/Pd(111) surface with femtosecond laser pulses can provide the possibility for a new reaction path, or a reaction channel favoured by TPD (desorption of CO and NO) which can be different from a reaction channel favoured by fs-LID (preferably CO and NO reaction).

1.10 Thesis outline

In this chapter, the theoretical concepts for Chapter 4 and 5 have been introduced.

Chapter 2 describes a novel apparatus designed for fs-LID studies, and describes in detail photodesorption experiments. Basic theoretical concepts for TPD and RAIRS are also described.

Chapter 3 describes the design and commissioning of a femtosecond extreme ultraviolet (XUV) source, and theoretical simulations of the 9th (89 nm) and the 11th (72 nm) harmonic of the fundamental 800 nm femtosecond radiation. This apparatus can currently be used for gas phase photochemistry experiments.

Chapter 4 describes fs-LID studies of CO and NO adsorbed individually on the Pd(111) surface. Fs-LID studies are performed for three CO (NO) exposures, respectively. These studies are accompanied by RAIRS and TPD, and provide a good test of the new apparatus.

In Chapter 5, fs-LID studies are presented for systems where CO and NO are co-adsorbed. Studies were performed either by first dosing NO and then exposing the surface to CO, or by first dosing CO and then exposing the surface to NO. The photodesorption behaviour of CO or NO in the co-adsorbed systems is compared with the photodesorption of pure CO or NO, respectively.

1.11 References

1. C. V. Shank, R. L. Fork, R. Yen, R. H. Stolen and W. J. Tomlinson, *Applied Physics Letters*, **40** (9), 761 (1982).
2. A. H. Zewail, *Angewandte Chemie-International Edition*, **39** (15), 2587 (2000).
3. D. R. Rainer, S. M. Vesecky, M. Koranne, W. S. Oh and D. W. Goodman, *Journal of Catalysis*, **167** (1), 234 (1997).
4. J. D. Butler and D. R. Davis, *Journal of the Chemical Society-Dalton Transactions*, (21), 2249 (1976).
5. S. H. Oh, G. B. Fisher, J. E. Carpenter and D. W. Goodman, *Journal of Catalysis*, **100** (2), 360 (1986).
6. L. M. Carballo, T. Hahn and H. G. Lintz, *Applied Surface Science*, **40** (1-2), 53 (1989).
7. T. Hahn and H. G. Lintz, *Applied Surface Science*, **40** (1-2), 59 (1989).

8. S. H. Oh and C. C. Eickel, *Journal of Catalysis*, **128** (2), 526 (1991).
9. B. K. Cho, *Journal of Catalysis*, **148** (2), 697 (1994).
10. K. Y. S. Ng, D. N. Belton, S. J. Schmieg and G. B. Fischer, *Journal of Catalysis*, **146** (2), 394 (1994).
11. M. Valden, J. Aaltonen, E. Kuusisto, M. Pessa and C. J. Barnes, *Surface Science*, **307**, 193 (1994).
12. C. Howitt, V. Pitchon and G. Maire, *Journal of Catalysis*, **154** (1), 47 (1995).
13. F. Gao, Y. L. Wang and D. W. Goodman, *Journal of Catalysis*, **268** (1), 115 (2009).
14. G. Ertl, *Reactions at Solid Surfaces* (Wiley, 2009).
15. I. Langmuir, *Transactions of the Faraday Society*, **17**, 607 (1922).
16. J. Misewich, J. H. Glownia, J. E. Rothenberg and P. P. Sorokin, *Chemical Physics Letters*, **150** (5), 374 (1988).
17. M. J. Rosker, M. Dantus and A. H. Zewail, *Science*, **241** (4870), 1200 (1988).
18. G. D. Billing, *Chemical Physics*, **116** (2), 269 (1987).
19. J. C. Tully, *Journal of Chemical Physics*, **93** (2), 1061 (1990).
20. M. Head-Gordon and J. C. Tully, *Journal of Chemical Physics*, **96** (5), 3939 (1992).
21. M. Head-Gordon and J. C. Tully, *Physical Review B*, **46** (3), 1853 (1992).
22. E. Hasselbrink, *Surface Science*, **270**, 235 (1992).
23. S. I. Anisimov, B. Kapeliovich and T. L. Perelman, *Zhurnal Eksperimentalnoi I Teoreticheskoi Fiziki*, **66** (2), 776 (1974).
24. A. P. Miller and B. N. Brockhouse, *Canadian Journal of Physics*, **49**, 720 (1971).
25. C. Kittel, *Introduction to Solid State Physics*. (Wiley, 1996).
26. A. P. Kanavin, I. V. Smetanin, V. A. Isakov, Y. V. Afanasiev, B. N. Chichkov, B. Wellegehausen, S. Nolte, C. Momma and A. Tunnermann, *Physical Review B*, **57** (23), 14698 (1998).
27. P. B. Allen, *Physical Review Letters*, **59** (13), 1460 (1987).
28. D. E. Gray, *American Institute of Physics Handbook* - 3rd ed. (McGraw-Hill, New York, 1972).
29. P. Szymanski, A. L. Harris, N. Camillone III, *Surface Science*, **601** (16), 3335 (2007).
30. G. Blyholder, *Journal of Physical Chemistry*, **68** (10), 2772 (1964).
31. B. Gumhalter, K. Wandelt and P. Avouris, *Physical Review B*, **37** (14), 8048 (1988).

32. P. Avouris and R. E. Walkup, *Annual Review of Physical Chemistry*, **40**, 173 (1989).
33. S. Ohnishi and N. Watari, *Physical Review B*, **49** (20), 14619 (1994).
34. F. Illas, S. Zurita and A. M. Marquez, *Surface Science*, **376** (1-3), 279 (1997).
35. M. Gajdos, A. Eichler and J. Hafner, *Journal of Physics-Condensed Matter*, **16** (8), 1141 (2004).
36. O. Krogh Andersen, *Physical Review B*, **2** (4), 883 (1970).
37. M. Gajdos, A. Eichler and J. Hafner, *Journal of Physics-Condensed Matter*, **18** (1), 13 (2006).
38. F. Delbecq, B. Moraweck and L. Verite, *Surface Science*, **396** (1-3), 156 (1998).
39. D. S. King and R. R. Cavanagh, *Advances in Chemical Physics*, **76**, 45 (1989).
40. D. M. Newns, T. F. Heinz and J. A. Misewich, *Progress of Theoretical Physics Supplement*, (106), 411 (1991).
41. M. Brandbyge, P. Hedegard and T. F. Heinz, *Physical Review B*, **52** (8), 6042 (1995).
42. S. Wagner, *State- and Time-Resolved Investigations of Energy Transfer Mechanisms in Femtosecond Laser Induced Associative Desorption*. (PhD Thesis, Berlin, 2006).
43. F. Budde, T. F. Heinz, A. Kalamarides, M. M. T. Loy and J. A. Misewich, *Surface Science*, **283** (1-3), 143 (1993).
44. L. M. Struck, L. J. Richter, S. A. Buntin, R. R. Cavanagh and J. C. Stephenson, *Physical Review Letters*, **77** (22), 4576 (1996).
45. H. Risken, *The Fokker-Planck Equation*. (Springer, 1989).
46. J. A. Misewich, T. F. Heinz and D. M. Newns, *Physical Review Letters*, **68** (25), 3737 (1992).
47. J. C. Tully and M. Head-Gordon, *Desorption Induced by Electronic Transitions DIET V*, eds. A. R. Burns, E. B. Stechel (Springer-Verlag, Berlin, 1993).
48. D. Menzel and R. Gomer, *Journal of Chemical Physics*, **41** (11), 3311 (1964).
49. P. A. Redhead, *Canadian Journal of Physics*, **42** (5), 886 (1964).
50. P. R. Antoniewicz, *Physical Review B*, 21, 3811 (1980)
51. C. Frischkorn and M. Wolf, *Chemical Reviews*, **106** (10), 4207 (2006).
52. F. J. Kao, D. G. Busch, D. Cohen, D. G. Dacosta and W. Ho, *Physical Review Letters*, **71** (13), 2094 (1993).

53. M. Bonn, S. Funk and C. Hess, *Science*, **285** (5430), 1042 (1999).

54. J. A. Prybyla, T. F. Heinz and J. A. Misewich, *Physical Review Letters*, **64** (13), 1537 (1990).

55. S. Funk, M. Bonn, D. N. Denzler, C. Hess, M. Wolf and G. Ertl, *Journal of Chemical Physics*, **112** (22), 9888 (2000).

56. P. Szymanski, A. L. Harris and N. Camillone III, *Journal of Physical Chemistry A*, **111** (49), 12524 (2007).